Received: 19 December 2024 | Revised: 22 January 2025 | Accepted: 23 January 2025

DOI: 10.1002/pen.27125

RESEARCH ARTICLE

POLYMER ENGINEERING AND SCIENCE WILEY

Preparation and characterization of an acrylated-coumarin-containing photo-crosslinked thiol-ene network: Investigation of the free-volume, thermal, UV, and photoluminescence properties

Fatmanur Uyumaz[1] | **Gamze Özgül Artuç**[2] | **Gamze Pehlivan**[3] | **Ayça Akdoğan**[3] | **Uğur Yahşi**[3] | **Cumali Tav**[3] | **Mustafa Bulut**[1] | **Memet Vezir Kahraman**[1]

[1]Department of Chemistry, Faculty of Science, Marmara University, Istanbul, Turkey

[2]Department of Chemical Engineering, Faculty of Engineering and Natural Sciences, Istanbul Health and Technology University, Istanbul, Turkey

[3]Department of Physics, Faculty of Science, Marmara University, Istanbul, Turkey

Correspondence
Memet Vezir Kahraman, Department of Chemistry, Faculty of Science, Marmara University, Istanbul 34722, Turkey.
Email: mvezir@marmara.edu.tr

Uğur Yahşi, Department of Physics, Faculty of Science, Marmara University, Istanbul 34722, Turkey.
Email: uyahsi@marmara.edu.tr

Funding information
Marmara University, Grant/Award Number: FEN-C-YLP-141112-0337

Abstract

Coumarin, a versatile compound, has attracted great interest in polymer science due to its unique properties and diverse applications. The use of coumarins in polymer research opens avenues for the development of materials with improved functionalities. In this study, an acrylated coumarin (a-coumarin) compound-containing polymeric films was obtained via UV curing through a thiol-ene click reaction with a free radical mechanism. The obtained a-coumarin-containing polymeric films were subjected to functional characterization using FTIR and NMR analyses and thermal characterization via DSC and TGA. UV–vis and PL analyses were performed to determine the optical properties. Using positron annihilation lifetime spectroscopy (PALS), the free volume and proportional free volume fraction of the films were analyzed both below and above the glass transition temperature (T_g). The T_g values obtained from PALS were several degrees lower than those obtained via DSC. A-coumarin additives inhibit segmental mobility, hence reducing the proportional free volume fraction and increasing the T_g. This study is the first in the literature to investigate the free volume properties of coumarin-containing polymeric films. The study reveals the impact of a-coumarin on thermal, optical, and free volume properties, paving the way for the design of advanced functional materials.

Highlights

- A-coumarin films were made via UV curing and thiol-ene click chemistry.
- PALS analyzed free volume below and above the glass transition temperature.
- A-coumarin reduced free volume, increasing T_g and stabilizing polymer films.

KEYWORDS

acrylated coumarin, free volume, free volume fraction, polymeric film, positron annihilation lifetime spectroscopy

1 | INTRODUCTION

A variety of naturally occurring, semisynthetic, and synthetically derived physiologically active chemicals have coumarin, also known as 2H-1-benzopyran-2-one, as their core structure.[1] It is a commercially important chromophore since it bears the parent nucleus of benzopyrone.[2] The metabolism of coumarin in humans has been thoroughly investigated, and both its natural presence and its numerous derivatives are of interest in many areas.[3] Coumarin has been used in the creation of light-responsive polymer systems within the field of polymer science. To produce materials with dynamic qualities that can change shape when exposed to light, coumarin and its derivatives have been incorporated into polymer architectures.[4] The characteristics such as UV responsiveness and viscoelastic behavior can be tuned by synthesizing star-shaped polymeric materials with acrylated coumarin (a-coumarin).[5,6] Applications, including tissue engineering, drug delivery systems, soft robotics, and 4D printing, have demonstrated potential for these materials.[7–9] Furthermore, to improve the fluorescence characteristics of materials, coumarin-based fluorescent monomers have been added to polymeric backbones.[10] The potential for coumarin-based fluorescent polymers in a variety of applications has been demonstrated by the copolymerization of 3-vinylcoumarins with other monomers.[10] Owing to its many characteristics and possible uses, methyl 2-(7-hydroxy-2-oxo-2H-chromen-4-yl) acetate has been the subject of much research. Many derivatives of this chemical with various biological activities and functions have been synthesized. For example, it has been used to create sol–gel materials with blue luminescence.[11]

Acrylate polymers are incredibly adaptable materials with a broad range of uses in many industries. These polymers are important in areas where durability is critical because of their remarkable mechanical qualities, which include high elasticity and resistance to breaking.[12] Acrylated polymers can be tailored to display desired characteristics by adding particular functional groups, which enables the construction of intricate macromolecular structures for a variety of uses.[13] The mechanical strength, transparency, and processability of acrylate polymers make them ideal for creating novel materials with specific functions for a wide range of applications. The moderate conditions, high efficiency, regioselectivity, adaptability, ease of post-treatment, and environmentally friendly nature of the thiol-ene click reaction make it an invaluable tool in many scientific areas. Its benefits and characteristics make it the material of choice for many applications, ranging from biomolecule functionalization to polymer chemistry and surface modifications.[14–16] The effect of free volume in polymers can explain important physical properties, including some thermodynamic properties such as the glass transition temperature,[17,18] gas permeability,[19,20] viscosity,[21–24] dielectric relaxation,[25,26] and ionic conductivity.[27–32]

In this study, N-vinyl pyrrolidone (NVP) works as a reactive diluent, lowering the viscosity of the formulation for easier handling and processing. It contributes to the polymerization process via its vinyl group, forming covalent bonds within the network to promote flexibility and durability.[33] Polyester diacrylate is a difunctional acrylate monomer that serves as a primary base resin. It provides mechanical strength and serves as the backbone of the polymer network when UV-cured.[34] Trimethylolpropane triacrylate (TMPTA) is a trifunctional acrylate monomer that works as a crosslinker, increasing the density of the polymer network. It improves the hardness, thermal stability, and chemical resistance of the material.[35] Pentaerythritol Tetrakis (3-Mercaptopropionate) is a tetrafunctional thiol that is involved in the thiol-ene reaction with acrylate monomers. It promotes the polymerization process and leads to the creation of a highly cross-linked, robust, and flexible network. Its unique thiol-ene reaction kinetics allow it to speed up the curing process and reduce shrinkage.[36]

Therefore, determining the free volume behavior of a-coumarin-containing thiol-ene polymeric films, in which coumarin is acrylated and polymerized and then UV-cured via a free radical mechanism, is crucial. The free volume changes resulting from the addition of different mass percentages of a-coumarin to the polymeric mixture were analyzed via PALS, a unique nondestructive method.

2 | EXPERIMENTAL

2.1 | Materials

2-Methylresorcinol, dimethyl 2-acetylsuccinate, sulfuric acid, triethylamine (TEA), tetrahydrofuran (THF), N-vinyl pyrrolidone (NVP), 2-hydroxy-2-methylpropiophenone (Darocur 1173), pentaerythritol tetrakis (3-mercaptopropionate)

(PETMP), and trimethylolpropane triacrylate (TMPTA) were purchased from Sigma Aldrich, Netherlands. Acryloyl chloride (AC) was purchased from Alfa Aesar, USA. Polyester diacrylate (PEDA) was obtained from Croda Chem, UK.

2.2 | Synthesis of coumarin

The coumarin compound (methyl 2-(7-hydroxy-4,-8-dimethyl-2-oxo-*2H*-chromen-3-yl) acetate) used in the synthesis of polymeric films was synthesized according to the Pechmann method described in the literature.[37–39] 2-Methylresorcinol (2 g, 16.11 mmol) and dimethyl 2-acetylsuccinate (3.032 g, 16.11 mmol) were dissolved in 15 mL% 98 H_2SO_4. The reaction mixture was stirred at 0–5°C for 4 h. The reaction mixture was subsequently poured into cold water. The crude product was filtered and washed with water until the acidity was removed. The product obtained was stored at room temperature for use in the next reaction (Figure 1).

2.3 | Synthesis of acrylated coumarin

After 1 g of coumarin (3.81 mmol) was dissolved in THF, 0.424 g (4.19 mmol) of triethylamine was added to the reaction flask. An ice bath was used to decrease the temperature of the solution to 0–5°C, and 0.379 g (4.19 mmol) of acryloyl chloride was added dropwise to the mixture over a duration of 15 min. The reaction was halted after 12 h, and the resulting salt was filtered to remove some of the solvent before it precipitated in water. The product was vacuum-dried at 30°C after being filtered as a white solid. The monomer was determined to have an 80% yield. Figure 2 displays the a-coumarin synthesis reaction.

2.4 | Preparation of polymeric films

First, 0.014 g (1 wt%) of synthesized a-coumarin was dissolved in 0.15 g of N-vinyl pyrrolidone. In another beaker, 0.65 g of polyester diacrylate and 0.20 g of trimethylolpropane triacrylate were mixed and stirred homogeneously at room temperature. Dissolved a-coumarin was added to the beaker and stirred. Darocur 1173 photoinitiator was added to the solution at 3 wt%. Finally, pentaerythritol tetrakis (3-mercaptopropionate) was added and mixed. The solution was poured into a Teflon mold and cured by exposure to UV light. The films, each approximately 1 mm thick and 1 × 3 cm in size, were demoulded after 3 min, and various characterizations were performed.

3 | CHARACTERIZATION

Fourier-transform infrared spectroscopy (FTIR) was performed using a Perkin Elmer Spectrum100 instrument (USA) to analyze the functional groups contained in the materials. The examination with FTIR includes a wide range of wavenumbers from 4000 to 400 cm^{-1}. ^{1}H-NMR spectroscopy with a Varian Mercury-VX 400 MHz BB instrument was used to analyze the detailed structure of the molecule and the chemical environment of the atoms. The thermal stability of the crosslinked films was examined via thermogravimetric analysis (TGA) on a Perkin Elmer 4000 (USA) apparatus. In a dry nitrogen environment, the measurements were conducted across a temperature range of 30–700°C with a heating rate of 20°C min^{-1}. Differential scanning calorimetry (DSC) measurements were performed on the polymeric films between −30 and 100°C using a Perkin Elmer Diamond DSC system. DSC analysis was conducted under a nitrogen atmosphere with a heating rate of 10°C min^{-1}. Optical spectra in the UV–vis range were

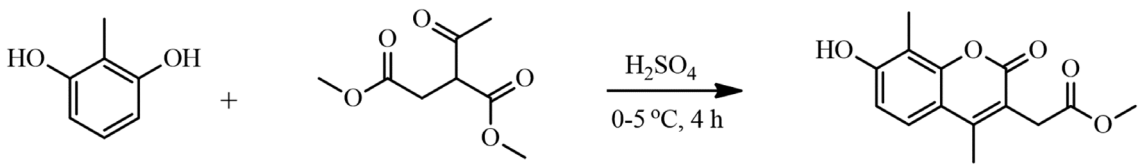

FIGURE 1 Synthesis of coumarin.

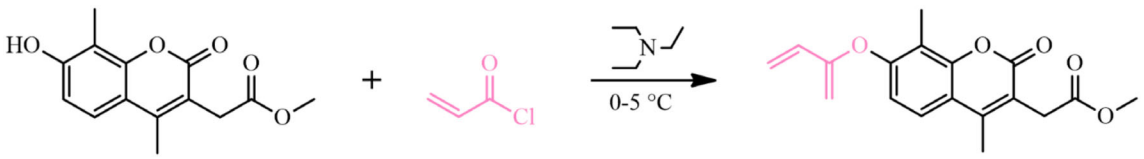

FIGURE 2 Synthesis of acrylated coumarin.

obtained via a Shimadzu 2450 UV–Vis spectrophotometer. On a Hitachi F-7000 spectrofluorometer, room temperature cuvettes with a 1 cm path length were used to record the emission and excitation spectra of fluorescence.

For PALS measurements, a positron source with a strength of approximately 25 μCi is obtained by evaporating ^{22}NaCl sources in the form of an aqueous solution encapsulated by two Kapton foils, each with a thickness of 7 μm. The source is sandwiched between two samples with thicknesses of approximately 2 mm, each consisting of two 1 mm thick pieces. The positron source emits a positron and an accompanied gamma-ray of 1274 keV called the "start signal." Upon entering the sample, a positron with a characteristic maximum energy of 546 keV thermalizes in the sample and localizes in an open space called the free volume. During this process, the positrons can undergo direct annihilation with electrons. However, when a positron interacts with an electron, it can form two states of positronium within a sufficient free volume: para-positronium (p-Ps), which is a singlet state with opposite spins, and ortho-positronium (o-Ps), which is a triplet state with parallel spins.[40] p-Ps has a very short lifetime of 0.125 ns in a vacuum, and its lifetime is not significantly affected by its interaction with the surrounding polymer.[37] On the other hand, o-Ps has a much longer lifetime of 142 ns in a vacuum. However, when the positron interacts with the surrounding electron in a free volume, the positron annihilates in the so-called pick-off exchange reaction, and this interaction noticeably reduces the lifetime of the o-Ps, which is related to the size of the cavity. The 511 keV gamma ray annihilation is seen as a stop signal. The PALS system operates on the basis of the temporal disparity between the start and stop signals.[41,42]

This technique is based on a fast–fast coincidence system. The PALS setup consists of the following components: (i) two ultrafast timing plastic scintillators (BC418) mounted on photomultiplier tubes (Hamamatsu R2059 PMT) coupled to two voltage dividers (Ortec 265) supplying −2050 Volts, (ii) two constant fraction differential discriminators (Ortec 583B CFDD) fed by the start and stop signals from the PMT used as a time signal generator filter within the selected energy ranges, (iii) a time-to-amplitude converter (Ortec 566 TAC), which converts the CFDD's time-marked signals into time-to-pulse-height signals, and (iv) a multichannel analyzer (Ortec ASPEC-927 MCA), which yields a spectrum of positron lifetimes.[43–46] When we obtain the signals from the MCA through the Maestro interface, we obtain the time graph (or time-calibrated channel number) of the lifetime spectrum. To reveal the lifetime parameters, a convolution program (called "LT polymer")[47] is used to decompose the lifetime spectrum into lifetimes and intensities of p-Ps (τ_1 and I_1), direct annihilation (τ_2 and I_2), and o-Ps (τ_3 and I_3). Here, the first terms in parentheses represent the lifetimes, and the second terms represent the intensities. The source contributions and resolution were determined via a Si crystal with a single lifetime of 0.22 ns. The source contribution (Kapton, NaCl, and adhesive gel) is 17.9%, with two lifetime components: 0.385 ns with 85.5% and 1.31 ns with 14.5%. The resolution of the system is approximately 350 ps, and a million counts were taken for each run.

To estimate the free volume size and free volume fraction from the o-Ps lifetime and intensity, a model for positronium (called "Tao-Eldrup")[48,49] is employed, in which this model assumes that positronium resides in an infinite spherical potential well of radius R. The Tao-Eldrup model relates τ_3 and R via the following equation[44,45]

$$\frac{1}{\tau_3} = 2\left(1 - \frac{R}{\Delta R + R} + \frac{1}{2\pi}\sin\frac{2\pi R}{\Delta R + R}\right), \quad (1)$$

where the surrounding spherical electron layer with thickness ΔR, which is approximately 0.1656 nm, is empirically obtained.[50,51] The free volume $v_f(\tau_3) = 4\pi R^3/3$ can be calculated via R from the numerical solution of Equation (1). For the free volume fraction (f_{vf}), Kobayashi et al.[52] offered a model that relates it to the free volume (v_f) and the o-Ps intensity (I_3) via

$$f_{vf} = CI_3 v_f(\tau_3), \quad (2)$$

where the constant C can be assigned a value compared with other means, such as using the hole fraction of the SS theory.[52–54] Owing to the lack of PVT data for these newly synthesized compounds, we utilize the product of I_3 and v_f as a measure of the free volume fraction, which we call the proportional free volume fraction.

4 | RESULTS AND DISCUSSION

Polymeric films were fabricated from solutions of polyester diacrylate, trimethylolpropane triacrylate, pentaerythritol tetrakis (3-mercaptopropionate), and a-coumarin, which were dissolved in NVP. The films were cured by UV radiation. After crosslinking, cross-linked films were created via a thiol–ene click reaction with free radical polymerization, and their chemical structure was investigated via FTIR spectroscopy. The thiol–ene click reaction allows for the rapid and efficient formation of stable thioether bonds under UV irradiation, providing a robust method for polymerization and material synthesis.[55] Furthermore, the thiol–ene click reaction has demonstrated excellent orthogonality under various reaction conditions,

making it a valuable tool in polymer chemistry.[56] To improve the physical properties of the polymeric film and observe the change in free volume, adjustments were made in the ratio of substrates and the amount of coumarin in the films (Table 1). This modification resulted in significant changes in the free volume ratio.

Figure 3 illustrates the formation of polymeric films via UV curing. This process involves crosslinking reactions between photosensitive PEDA, TMPTA, PETMP, and a-coumarin through UV radiation. To enhance the physical properties of the polymeric film, the ratio of the films was optimized, and all formulations are given in Table 1. This ratio is experimentally optimized to achieve the desired property balance.

A-Coumarin was obtained by the acrylation of coumarin with acryloyl chloride and triethyl amine. The coincident FTIR spectra of coumarin and a-coumarin are shown in Figure 4A. The OH peak observed at 3155 cm^{-1} in the coumarin spectrum disappeared after acrylation. The peaks at 2943 and 2954 cm^{-1} in both spectra are due

TABLE 1 Formulation of polymeric films.

	Polyester diacrylate	Trimethylolpropane triacrylate	N-Vinyl pyrrolidone	Pentaerythritol tetrakis(3-mercaptopropionate)	A-Coumarin
F0	0.65 g	0.20 g	0.15 g	0.4 g	-
F1	0.65 g	0.20 g	0.15 g	0.4 g	1 wt%
F2	0.65 g	0.20 g	0.15 g	0.4 g	3 wt%
F3	0.65 g	0.20 g	0.15 g	0.4 g	5 wt%

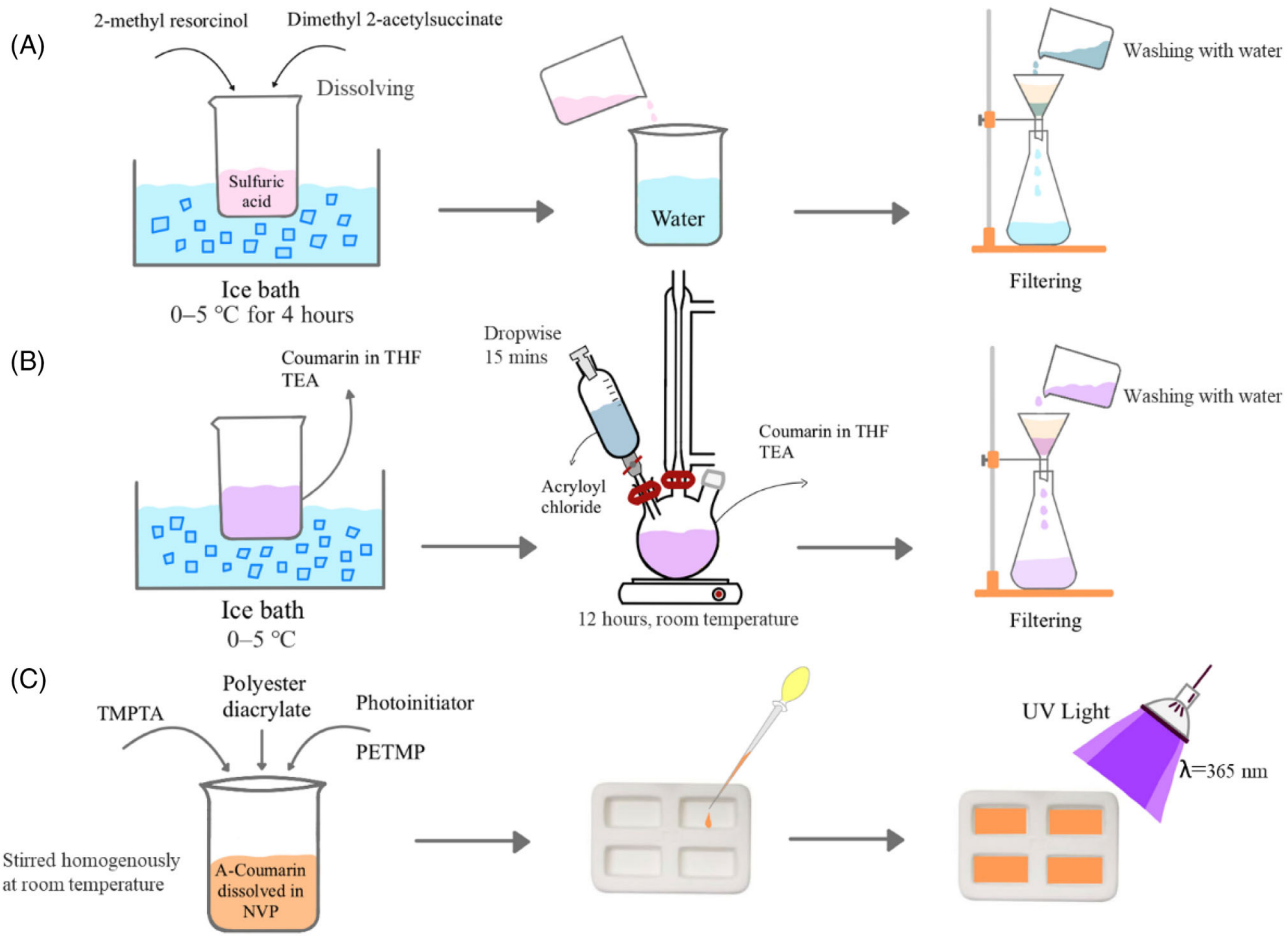

FIGURE 3 Schematic representation of (A) the synthesis of coumarin, (B) the synthesis of a-coumarin, and (C) the preparation of UV-cured crosslinked polymeric films. NVP, N-vinyl pyrrolidone; PETMP, pentaerythritol tetrakis (3-mercaptopropionate); TEA, triethylamine; TMPTA, trimethylolpropane triacrylate.

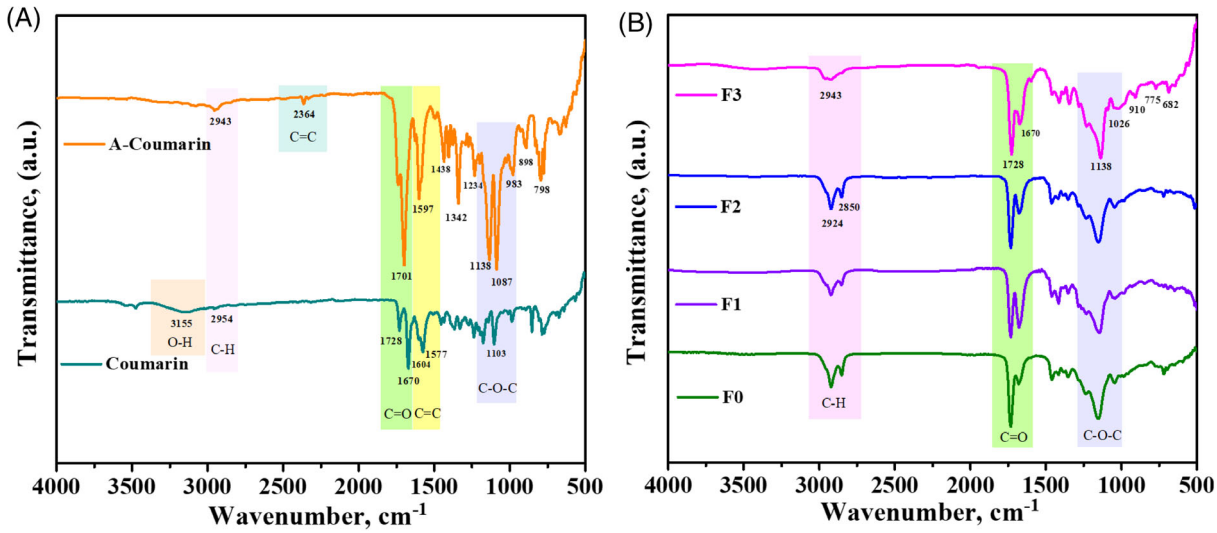

FIGURE 4 Fourier-transform infrared spectroscopy results of (A) coumarin and a-coumarin (B) polymeric films.

to C—H deformations in the CH_2 and CH_3 groups of C-coumarin and a-coumarin. The carbonyl group vibration observed at 1670 cm^{-1} shifted to 1701 cm^{-1} after the acceleration reaction. The peaks observed at 1577 and 1597 cm^{-1} are attributed to C═C double bonds. The peak at 2364 cm^{-1} in the a-coumarin spectrum is attributed to the C═C double bond of the acrylate group. Moreover, the peak observed at 798 cm^{-1} indicates that the acrylate group is covalently bonded to the structure. In addition, vibrations of ester groups were observed at 1103 and 1087 cm^{-1}. Overall, the FTIR peaks obtained from the film can serve as valuable indicators of the molecular composition and bonding characteristics resulting from the polymerization process. As shown in the FTIR spectra in Figure 4B, the peaks observed at 2924–2850 cm^{-1} and 2943 cm^{-1} in all the spectra are due to C—H deformations in the CH_2 and CH_3 groups. The C═O stretching peak was observed at 1728 cm^{-1}. The disappearance of the C═C peak at 2364 cm^{-1} in the polymeric film spectrum proves the occurrence of the thiol-ene click reaction and the presence of a crosslinked structure.[57]

Figure 5 displays the ^{1}H-NMR spectrum of acrylated coumarin. The ^{1}H NMR spectrum of the acrylated coumarin compound reveals distinct signals corresponding to its structural features. In the aliphatic region, the peak at 2.2 ppm (a) is attributed to the methyl protons adjacent to the coumarin ring, appearing as a singlet due to the absence of neighboring protons. The signal at 2.7 ppm (b) corresponds to methoxy protons on the coumarin structure, also a singlet. The methylene protons in the acrylate chain are observed at 3.9 ppm (d), likely appearing as a triplet due to coupling with adjacent protons. In the aromatic region, vinyl protons of the acrylate group appear between 6.1 and 6.5 ppm[58] (e, f, g), showing splitting patterns such as doublets and doublet of doublets, consistent with their couplings. The aromatic protons of the coumarin core resonate between 7.0 and 7.8 ppm (h, i), displaying doublets and multiplets due to interactions within the conjugated system. These peaks confirm the successful incorporation of the acrylate functionality and the characteristic coumarin structure.

The phase transition temperatures were measured via differential scanning calorimetry (DSC) at a heating rate of 10°C min^{-1} in a nitrogen (N_2) environment. Two heat cycles in hermetically sealed aluminum pans covering a temperature range of −10–100°C were used for the DSC investigations. The midpoint of the gradual shift that takes place during the second heating cycle was determined to be the glass transition temperature (T_g) (Figure 6A). In this case, high T_g values may result from the anticipated impact of a significant cross-linked network.[59] As a result, low T_g values promote segmental mobility while decreasing crystallization.[60] Thus, the T_g values for the F0, F1, F2, and F3 films were 75.2, 79.5, 84.6, and 86.9°C, respectively. Reorganization of the polymer chains or relaxation of trapped stresses in the polymer network can release heat during heating, which is shown as an exothermic peak in F0 sample.[61] The absence of a-coumarin in F0 may also explain the exothermic peak, since a-coumarin may act as a stabilizer or modifier in other formulations (F1, F2, F3), preventing such exothermic processes.[62]

Polymers must be thermally stable for use in a variety of applications. Thermogravimetric analysis (TGA) was performed at a heating rate of 20°C min^{-1} in the temperature range of 30–700°C in a nitrogen environment to assess the thermal stability of the polymeric films. TGA curves of the films are displayed in Figure 6B. The

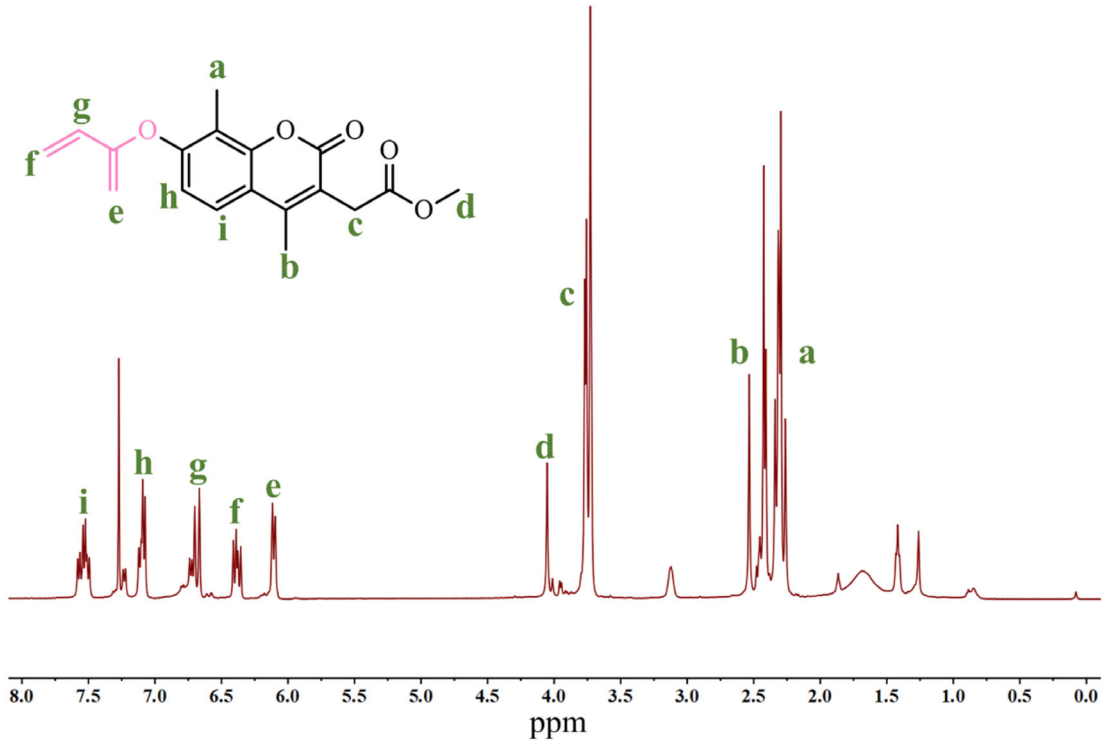

FIGURE 5 ^{1}H-NMR spectra of acrylated coumarin.

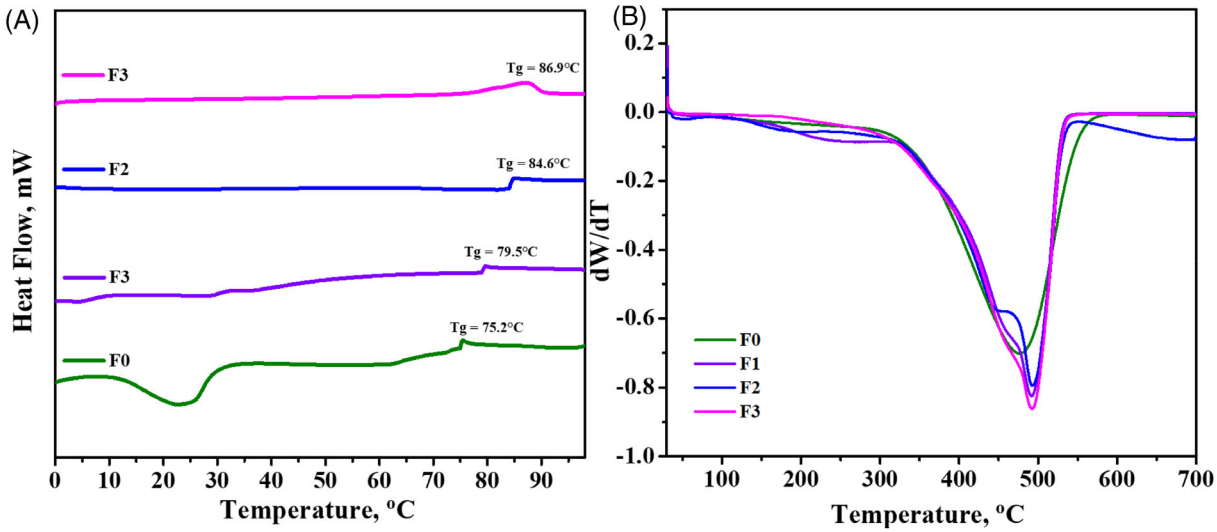

FIGURE 6 (A) Differential scanning calorimetry results and (B) thermogravimetric analysis (dW/dT) results of the polymeric films.

observed decrease in weight, which ranged from 1.5% to 5% for each of the samples below 200°C, was attributed to the elimination of volatile substances included in the polymer matrix. The F3 sample, which contains 3% a-coumarin, has the highest decomposition temperature. The strongly cross-linked structure is responsible for both this difference and the increased thermal stability. The weight loss in polymeric films, which approaches 6%–13% in the 200–300°C temperature range, is caused by the evaporation of both bound and unbound water molecules present in the structure. It was concluded that primary degradation started at approximately 300°C. The outstanding thermal stability of the polymeric films is supported by all of these findings.

UV–Vis and fluorescence spectroscopy can be used to characterize coumarins since they emit and absorb light in the UV–visible range. Typically, the violet region (300–400 nm) is where one can observe the unique bands

of coumarins. A-coumarin-bound polymeric film samples were measured via thin filming on glass and referenced against air. Absorption bands were observed at 285 nm for F0, 288 nm for F1, 293 nm for F2 and 303 nm for F3. The UV spectrum of the polymeric films shifted to 5–10 nm red with the addition of the a-coumarin compound. The redshift observed in the UV–vis spectra of the polymeric films with the addition of the a-coumarin compound is attributed to the increase in the number of chromophore groups in the compound as the percentage of coumarin increases.[63] A-coumarin-containing polymeric film has high fluorescence emission (Figure 7B). The emission bands of the films were observed at 380 nm for F0, 383 nm for F1, 387 nm for F2, and 390 nm for the F3 film ($\lambda^{em}_{start} = 335$ nm). Similarly, a shift toward the red region was observed with an increasing number of chromophore groups.

The PALS analysis of polymeric films containing a-coumarin at different mass percentages was performed via LT-Polymers because their lifetimes and intensities fixed the p-Ps lifetime at 0.125 ns across temperatures ranging from 20 to 120°C. The direct annihilation parameters τ_2 and I_2, with ranges of 0.311–0.406 ns and 61%–66%, respectively, are not disclosed herein. We calculate the free volume radius via Equation (1) and the proportional free volume fraction $I_3 v_f$. In Figure 8A–C, the o-Ps lifetime (τ_3) (the corresponding free volume on the right vertical axis), o-Ps intensity (I_3), and proportional free volume fraction ($I_3 v_f$) are illustrated with respect to the temperature. The o-Ps lifetime (or the free volume) and the proportional free volume fraction increase with increasing temperature up to the derived T_g values, after which they remain approximately the same as the temperature increases further. In other words, the rate at which τ_3 changes with temperature falls in the region above the T_g relative to that below the T_g. This cross-linking restricts the mobility of the polymer segments, inhibiting free volume expansion beyond the T_g. Similar behavior was noted in cross-linked amorphous polyurethane[64] amine-cured epoxy polymer, the free-volume microstructure of glycerol[65] and our prior investigation of cross-linked thiol-ene networks.[45] From the proportional free volume fraction in Figure 8C, we estimated the T_g values to be 74, 77, 81, and 84°C for F0, F1, F2, and F3, respectively. To avoid confusion, we have only shown the T_g values for F0 and F3 in Figure 8C. Compared with the DSC measurements in Figure 6A, the PALS results are a few degrees lower. The increase in the glass transition temperature (T_g) observed when the weight percentage of a-coumarin was increased in the polymeric films can be attributed to the elevated melting temperature of a-coumarin. The mobility of the polymer segment inside the network is the main factor influencing the glass transition temperature (T_g) in relation to the free volume. A-Coumarin decreases the proportional free volume fraction in the polymer film network and restricts the movement of segments, resulting in an increase in the glass transition temperature (T_g).

Moreover, Figure 8B shows a nearly linear relationship between the o-Ps intensity and temperature, which is proportional to the number of available free volume sites. We attribute the expansion of the free volume in crosslinked films to its temperature-dependent increase up to the T_g value, after which it reaches a limit. However, the increase in the intensity above the T_g indicates that certain bonds within the cell network break up thermally to accommodate the additional free volume sites. In addition, as shown in Figure 8B, the o-Ps intensity decreases from

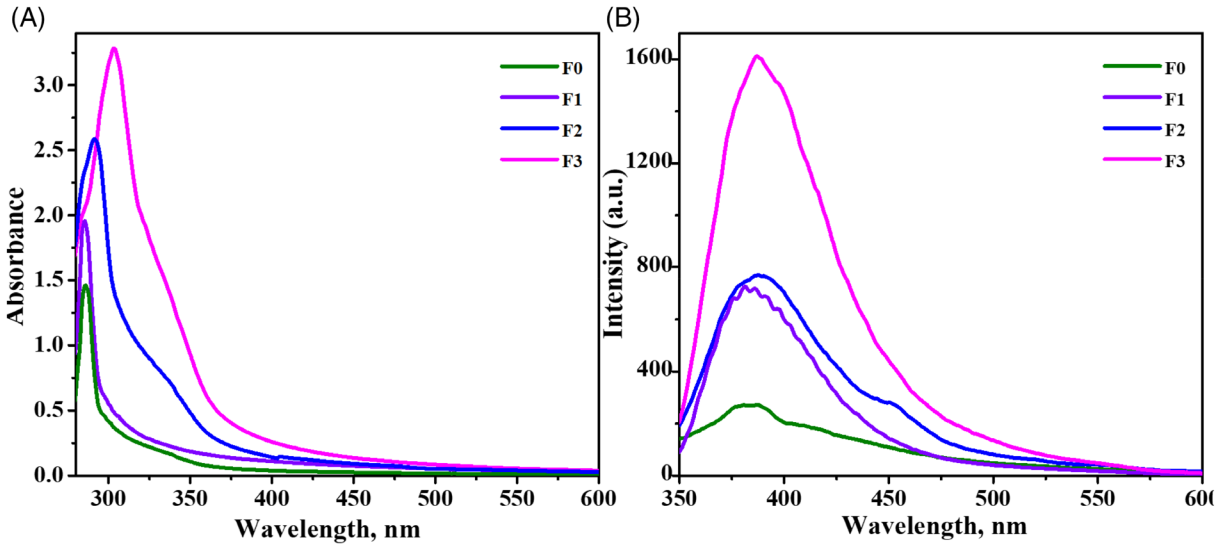

FIGURE 7 (A) UV–vis spectra and (B) PL spectra of the polymeric films.

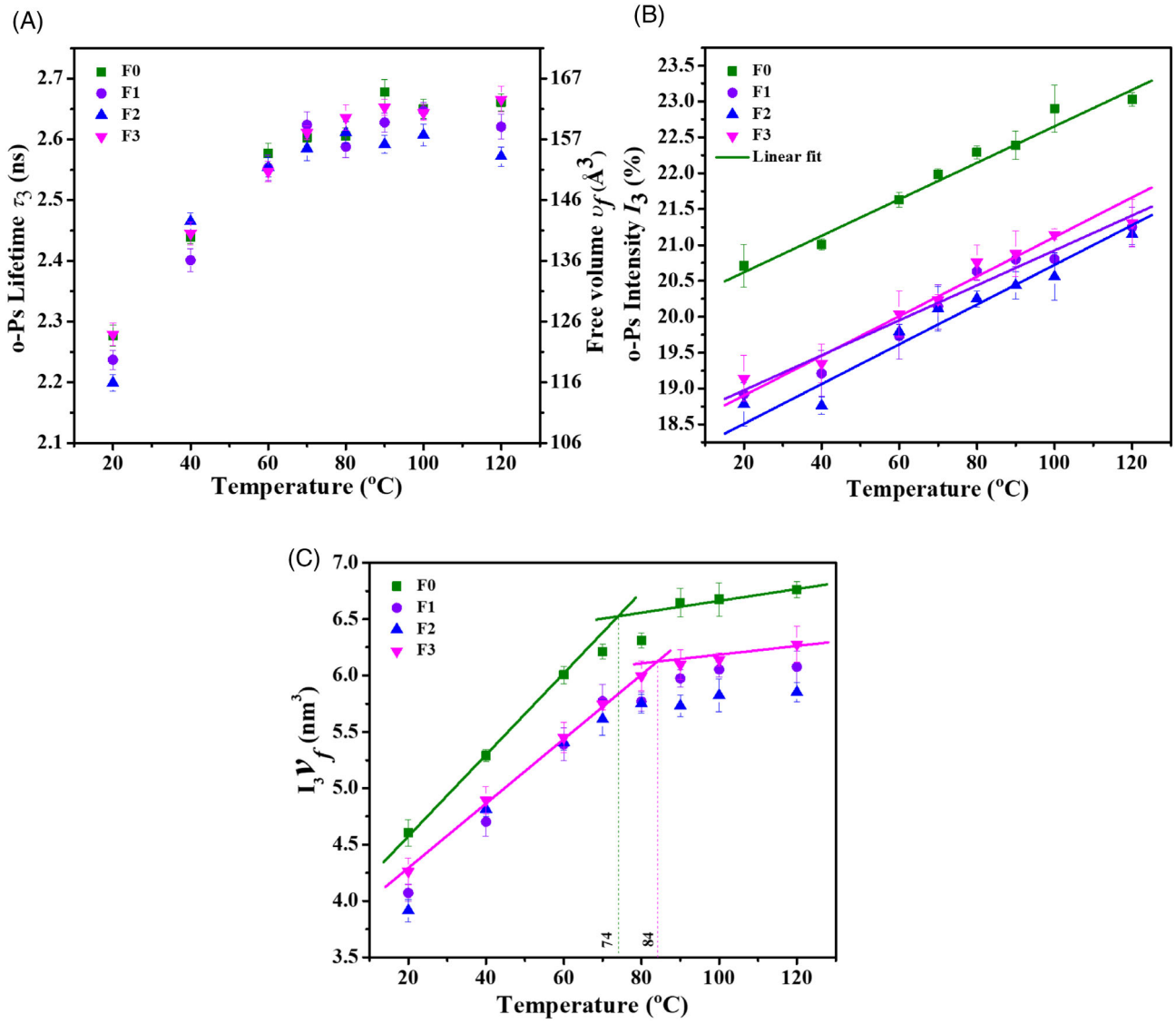

FIGURE 8 (A) o-Ps lifetime (τ_3) (or the corresponding free volume on the right axis), (B) o-Ps intensity (I_3), and (C) $I_3 v_f$ versus temperature for the samples.

20.7% for F0 to approximately 19.0% in the presence of a-coumarin (F1, F2, and F3) at 20°C. Increasing the a-coumarin concentration reduces the intensity up to 3 wt % but enhances it at 5 wt%, almost within the error bars for the range of temperatures. The integration of the a-coumarin into the polymer matrix results in alterations to the polymer's chain conformation and arrangement.[66] The reduction in I_3 and the free volume associated with a-coumarin inclusion is evident in structural compression and a diminished degree of disorder.

5 | CONCLUSION

A new acrylate polymeric film containing a coumarin group was synthesized via a UV curing method via a thiol-en click reaction. FTIR and NMR analyses were performed to characterize the functional groups. TGA and DSC analyses were performed to determine the thermal properties of the polymer. DSC analysis revealed that as the a-coumarin content in the formulation increased, the crosslink density increased, and the T_g increased. As a result of the PALS measurements, we conclude that the expansion of the free volume of the cross-linked films increases to approximately some T_g values, beyond which it becomes constant owing to its limits; however, the intensity increases, suggesting that the cell network breaks links to access a new free volume. Hence, the T_g values match the DSC results, albeit a few degrees lower. On the basis of the TGA results, the films have excellent thermal stability, making them suitable for a wide range of applications. Although the TGA thermal stability

curves are directly associated with the quantity of a-coumarin present, we established a correlation with the free volume. UV–vis and PL analyses were performed to determine the optical properties. With increasing coumarin content, a shift to the red region was observed due to the increasing number of chromophore groups. This innovative work has significant potential for breakthrough applications in advanced materials design. By incorporating acrylated coumarin (a-coumarin) into polymeric films, the study demonstrates its ability to modulate thermal and optical properties, reduce free volume fractions, and increase glass transition temperatures. These properties promise advances in the development of functional materials for optoelectronic applications such as photonic devices, light-emitting diodes, and UV sensors due to the unique fluorescent and optical properties of coumarin. Furthermore, the investigation of free volume properties using PALS brings a new approach to the design of materials with controlled permeability, paving the way for applications in gas separation membranes and energy storage systems. By improving our understanding of the effect of coumarin on polymer networks, this work provides a basis for creating a new generation of smart materials tailored for a variety of industrial and technological uses.

ACKNOWLEDGMENTS

This work was supported by the Marmara University, Scientific Research Projects Committee, under Grant FEN-C-YLP-141112-0337.

CONFLICT OF INTEREST STATEMENT

The authors declare that they have no competing interests.

DATA AVAILABILITY STATEMENT

The data that supports the findings of this study are available in the supplementary material of this article.

ORCID

Cumali Tav https://orcid.org/0000-0002-6500-7903
Memet Vezir Kahraman https://orcid.org/0000-0003-1043-6476

REFERENCES

1. Todorov LT, Kostova IP. Coumarin-transition metal complexes with biological activity: current trends and perspectives. *Front Chem*. 2024;12:12. doi:10.3389/fchem.2024.1342772
2. Zeng RF, Lan JS, Li XD, et al. A fluorescent coumarin-based probe for the fast detection of cysteine with live cell application. *Molecules*. 2017;22:1618. doi:10.3390/molecules22101618
3. Leonart L, Gasparetto J, Pontes F, Cerqueira L, De Francisco T, Pontarolo R. New metabolites of coumarin detected in human urine using ultra performance liquid chromatography/quadrupole-time-of-flight tandem mass spectrometry. *Molecules*. 2017;22:2031. doi:10.3390/molecules22112031
4. Jiang J, Shu Q, Chen X, et al. Photoinduced morphology switching of polymer nanoaggregates in aqueous solution. *Langmuir*. 2010;12:14247-14254. doi:10.1021/la102771h
5. Cazin I, Rossegger E, De La Cruz GG, Griesser T, Schlögl S. Recent advances in functional polymers containing coumarin chromophores. *Polymers*. 2020;25:56. doi:10.3390/polym13010056
6. Honda S, Tanaka N, Toyota T. Synthesis of star-shaped poly(n-butyl acrylate) oligomers with coumarin end groups and their networks for a UV-tunable viscoelastic material. *J Polym Sci Part A Polym Chem*. 2017;19:9-15. doi:10.1002/pola.28777
7. Shie MY, Shen YF, Astuti SD, et al. Review of polymeric materials in 4D printing biomedical applications. *Polymers*. 2019;12:1864. doi:10.3390/polym11111864
8. Stewart S, Domínguez-Robles J, Donnelly R, Larrañeta E. Implantable polymeric drug delivery devices: classification, manufacture, materials, and clinical applications. *Polymers*. 2018;12:1379. doi:10.3390/polym10121379
9. Teixeira E, Lima J, Parola A, Branco P. Incorporation of coumarin-based fluorescent monomers into co-oligomeric molecules. *Polymers*. 2018;3:396. doi:10.3390/polym10040396
10. Wu DT, Munguia-Lopez JG, Cho YW, et al. Polymeric scaffolds for dental, oral, and craniofacial regenerative medicine. *Molecules*. 2021;22:7043. doi:10.3390/molecules26227043
11. Ahmed G, Petkov I, Gutzov S. Optical properties of sol-gel materials doped with ethyl 2-(7-hydroxy-2-oxo-2H-chromen-4-yl) acetate. *Eur J Chem*. 2010;31:259-261. doi:10.5155/eurjchem.1.4.259-261.187
12. Laki S, Shamsabadi AA, Riazi H, Grady MC, Rappe AM, Soroush M. Experimental and mechanistic modeling study of self-initiated high-temperature polymerization of ethyl acrylate. *Ind Eng Chem Res*. 2019;27:2621-2630. doi:10.1021/acs.iecr.9b05050
13. Barner-Kowollik C. Acrylate free radical polymerization: from mechanism to polymer design. *Macromol Rapid Commun*. 2009;16:1961-1963. doi:10.1002/marc.200900676
14. Fu Q, Yan Q, Zhou M, Xie W, Fu H. Study on UV/sunlight curable self-healing topological polysulfide polymer network based on disulfide exchange. *Polymers Adv Technol*. 2021;21:2252-2261. doi:10.1002/pat.5259
15. Pan C, Liu P. Surface modification of attapulgite nanorods with nitrile butadiene rubber via thiol–Ene interfacial click reaction: grafting or crosslinking. *Ind Eng Chem Res*. 2018;22:4949-4954. doi:10.1021/acs.iecr.8b00094
16. Tian L, Ren G, Zhang P, et al. Preparation of fluorine-free waterproof and breathable electrospun nanofibrous membranes via thiol-ene click reaction. *Macromol Mater Eng*. 2022;307(4):2100757. doi:10.1002/mame.202100757
17. Bamford D, Dlubek G, Reiche A, et al. The local free volume, glass transition, and ionic conductivity in a polymer electrolyte: a positron lifetime study. *J Chem Phys*. 2001;15:7260-7270. doi:10.1063/1.1402633
18. Yu Z, Yahsi U, McGervey JD, Jamieson AM, Simha R. Molecular weight-dependence of free volume in polystyrene studied by positron annihilation measurements. *J Polym Sci B*. 1994;1:2637-2644. doi:10.1002/polb.1994.090321609
19. Mohamed HFM, Kobayashi Y, Kuroda CS, Takimoto N, Ohira A. Free volume, oxygen permeability, and uniaxial compression storage modulus of hydrated biphenol-based sulfonated poly(arylene ether sulfone). *J Membr Sci*. 2010;11:84-89. doi:10.1016/j.memsci.2010.05.003

20. Mohamed HFM, Ohira A, Kobayashi Y. Free volume and oxygen permeability in polymers related to polymer electrolyte fuel cells. *Mater Sci Forum*. 2009;607:58-60.
21. Sahin-Dinc F, Sorrentino A, Tav C, Yahsi U. The effect of hole fraction on viscosity in atactic and syndiotactic polystyrenes. *Int J Thermophys*. 2015;1:3239-3254. doi:10.1007/s10765-015-1990-4
22. Utracki LA, Sedlacek T. Free volume dependence of polymer viscosity. *Rheologica Acta*. 2006;46(4):479-494. doi:10.1007/s00397-006-0133-z
23. Yahsi U. Viscous behavior of linear and three-branch alkanes: linking the equilibrium and transport theories. *J Polym Sci B*. 1999;37:879-887. doi:10.1002/(SICI)1099-0488(19990501)37:9%3C879::AID-POLB2%3E3.0.CO;2-P
24. Sahin F, Yahsi U. Linking the viscous and vacancy behavior of high molecular weight hydrocarbons. *Rheol Acta*. 2004;1:159-167. doi:10.1007/s00397-003-0330-y
25. Yahsi U, Coskun B, Yumak A, Boubaker K, Tav C. Relaxation time of polypropylene glycol and polypropylene glycol dimethylether-like polymers in terms of fluid-phase temperature and pressure dependent hole fraction. *Eur Polym J*. 2015;2:226-232. doi:10.1016/j.eurpolymj.2015.04.038
26. Yahsi AY, Almashayek A, Yahsi U. Dielectric relaxation time of PVAc in terms of hole fraction calculated from the theory of Simha-Somcynsky. *Polymer*. 2024;1:126753. doi:10.1016/j.polymer.2024.126753
27. Abdel-Hady EE, Mohamed HFM. Microstructure changes of poly(vinyl chloride) investigated by positron annihilation techniques. *Polym Degrad Stab*. 2002;1:449-456. doi:10.1016/s0141-3910(02)00102-7
28. Bakar R, Darvishi S, Aydemir U, et al. Decoding polymer architecture effect on ion clustering, chain dynamics, and ionic conductivity in polymer electrolytes. *ACS Appl Energy Mater*. 2023;23:4053-4064. doi:10.1021/acsaem.3c00310
29. Mohamed HFM, Abdel-Hady EE, Mohamed SS. Temperature dependence of the free volume in polytetrafluoroethylene studied by positron annihilation spectroscopy. *Radiat Phys Chem*. 2006;5:160-164. doi:10.1016/j.radphyschem.2006.03.026
30. Ulutaş K, Yahsi U, Deligöz H, et al. Dielectric properties and conductivity of PVdF-co-HFP/LiClO4polymer electrolytes. *Can J Phys*. 2018;20:786-791. doi:10.1139/cjp-2017-0678
31. Yahsi U, Deligöz H, Tav C, et al. Ionic conductivity of PVdF-co-HFP/LiClO4in terms of free volume defects probed by positron annihilation lifetime spectroscopy. *Radiat Eff Defects Solids*. 2018;4:214-228. doi:10.1080/10420150.2018.1552959
32. Yahsi U, Ulutas K, Tav C, Deger D. On the ionic conductivity of polymer electrolytes in terms of hole fraction. *J Polym Sci B*. 2008;11:2249-2254. doi:10.1002/polb.21556
33. Cho YH, Kim BK. Electro-optic properties of CO_2 fixed-polymer/nematic LC composite films. *J Appl Polym Sci*. 2001;81:2744-2753. doi:10.1002/app.1720
34. Choi Y, Yoon J, Kim J, Lee C, Oh JS, Cho N. Development of bisphenol-a-glycidyl-methacrylate- and trimethylolpropane-triacrylate-based stereolithography 3D printing materials. *Polymers*. 2022;14:5198. doi:10.3390/polym14235198
35. Johnson A, Caudill CL, Tumbleston JR, et al. Single-step fabrication of computationally designed microneedles by continuous liquid interface production. *PLoS One*. 2016;11:e0162518. doi:10.1371/journal.pone.0162518
36. Uyumaz F, Nurgaziyeva E, Kalybekkyzy S, Kahraman MV. Thiol-ene photo crosslinked PUA-PUMA-based flexible gel polymer electrolyte for lithium-ion batteries. *Macromol Mater Eng*. 2024;309(7):2400051. doi:10.1002/mame.202400051
37. Dong J, Li K, Hong Z, et al. Design, synthesis and fungicidal evaluation of novel psoralen derivatives containing sulfonohydrazide or acylthiourea moiety. *Mol Divers*. 2022;6(27):571-588. doi:10.1007/s11030-022-10402-y
38. Lee S, Cil O, Haggie PM, Verkman AS. 4,8-Dimethylcoumarin inhibitors of intestinal anion exchanger slc26a3 (downregulated in adenoma) for anti-absorptive therapy of constipation. *J Med Chem*. 2019;7:8330-8337. doi:10.1021/acs.jmedchem.9b01192
39. Sequeira L, Distinto S, Meleddu R, et al. 2H-chromene and 7H-furo-chromene derivatives selectively inhibit tumour associated human carbonic anhydrase IX and XII isoforms. *J Enzyme Inhib Med Chem*. 2023;38(1):2270183. doi:10.1080/14756366.2023.2270183
40. Jean YC, Sandreczki TC, Ames DP. Positronium annihilation in amine-cured epoxy polymers. *J Polym Sci Part B Polym Phys*. 1986;1:1247-1258. doi:10.1002/polb.1986.090240605
41. Jean YC, Mallon PE, Schrader DM. *Principles and Applications of Positron and Positronium Chemistry*. WORLD SCIENTIFIC eBooks; 2003. doi:10.1142/5086
42. Soykan U, Khaleel M, Cetin S, Yahsi U, Tav C. Investigation of the relation between free volume and physico-mechanical performance in rigid polyurethane foam containing Turkey feather fibers: part 2. *J Cell Plast*. 2022;1:893-915. doi:10.1177/0021955x221144541
43. Akay LN, Kalkandelen C, Akti N, et al. Effects of sintering and zirconmullite doping on nanostructural vacancies of bovine hydroxyapatite by positron techniques. *J Am Ceram Soc*. 2023;13:3220-3227. doi:10.1111/jace.18985
44. Akay LN, Kuzec S, Akti N, et al. Investigation of Nd3+: Y2Si2O7 phosphors using photoluminescence and positron annihilation lifetime spectroscopy. *ECS J Solid State Sci Technol*. 2023;12:086005.
45. Beyler Cigil A, Madakbaş S, Tav C, Yahşi U, Kahraman MV. Free volume, thermal and morphological properties of photo-crosslinked thiol-Ene/nanodiamond hybrid network. *Pigment Resin Technol*. 2020;18:113-120. doi:10.1108/prt-05-2020-0045
46. Dumludag F, Yener MY, Basturk E, et al. Effects of boron nitrite in thermoplastic polyurethane on thermal, electrical and free volume properties. *Polym Bull*. 2018;2:4087-4101. doi:10.1007/s00289-018-2560-2
47. Kansy J. Microcomputer program for analysis of positron annihilation lifetime spectra. *Nucl Instrum Methods Phys Res Sect A*. 1996;1:235-244. doi:10.1016/0168-9002(96)00075-7
48. Eldrup M, Lightbody D, Sherwood JN. The temperature dependence of positron lifetimes in solid pivalic acid. *Chem Phys*. 1981;1:51-58. doi:10.1016/0301-0104(81)80307-2
49. Tao SJ. Positronium annihilation in molecular substances. *J Chem Phys*. 1972;1:5499-5510. doi:10.1063/1.1677067
50. Nakanishi H, Ujihira Y. Application of positron annihilation to the characterization of zeolites. *J Phys Chem*. 1982;1:4446-4450. doi:10.1021/j100219a035
51. Nakanishi H, Wang SJ, Jean YC, Sharama SC. *Positron Annihilation Studies of Fluids*. World Scientific; 1988:292-298.
52. Kobayashi Y, Zheng W, Meyer EF, McGervey JD, Jamieson AM, Simha R. Free volume and physical aging of

poly(vinyl acetate) studied by positron annihilation. *Macromolecules*. 1989;1:2302-2306. doi:10.1021/ma00195a052

53. Kaya A, Kösem G, Yener M, Tav C, Yahsi U, Esmer K. Structural and dielectrical properties of PMMA/TiO_2 composites in terms of free volume defects probed by positron annihilation lifetime spectroscopy. *Polym Polym Compos*. 2020;17:107-116. doi:10.1177/0967391120903533
54. Kuzeci S, Ozcan E, Kaya AU, et al. Free-volume analysis of the structural and dielectric properties of PMMA/TeO2 composites via positron annihilation lifetime spectroscopy. *J Alloys Compd*. 2024;1004:175938.
55. Zhang J, Aydogan C, Patias G, et al. Polymerization of myrcene in both conventional and renewable solvents: postpolymerization modification via regioselective photoinduced thiol–ene chemistry for use as carbon renewable dispersants. *ACS Sustain Chem Eng*. 2022;11:9654-9664. doi:10.1021/acssuschemeng.2c03755
56. Monfared M, Nothling MD, Mawad D, Stenzel MH. Effect of cell culture media on photopolymerizations. *Biomacromolecules*. 2021;22:4295-4305. doi:10.1021/acs.biomac.1c00864
57. Rahman ML, Ting TX, Sarjadi MS, et al. Synthesis of bent-shaped azobenzene main-chain polymers for photo-switching properties. *J Macromol Sci Part A*. 2023;5(61):40-52. doi:10.1080/10601325.2023.2287033
58. Ecochard Y, Auvergne R, Boutevin B, Caillol S. Linseed oil-based thermosets by Aza-Michael polymerization. *Eur J Lipid Sci Technol*. 2019;29:122. doi:10.1002/ejlt.201900145
59. Neagu C, Mihalcea L, Enachi E, et al. Cross-linked microencapsulation of CO_2 supercritical extracted oleoresins from sea buckthorn: evidence of targeted functionality and stability. *Molecules*. 2020;23:2442. doi:10.3390/molecules25102442
60. Xue Z, He D, Xie X. Poly(ethylene oxide)-based electrolytes for lithium-ion batteries. *J Mater Chem A*. 2015;1:19218-19253. doi:10.1039/c5ta03471j
61. Song H, Medvedev GA, Caruthers JM. Effect of anisotropic deformation on the differential scanning calorimetry response of polymer glasses. *J Polym Sci*. 2023;62:508-516. doi:10.1002/pol.20230631
62. Bian Y, Leng X, Wei Z, et al. End-chain fluorescent highly branched poly(l-lactide)s: synthesis, architecture-dependence, and fluorescent visible paclitaxel-loaded microspheres. *Biomacromolecules*. 2019;20:3952-3968. doi:10.1021/acs.biomac.9b01020
63. Vijay P, Batchelor W, Saito K. Preparation of coumarin polymer grafted nanocellulose films to form high performance, photoresponsive barrier layers. *J Polym Sci*. 2022;3:3447-3462. doi:10.1002/pol.20220248
64. Consolati G, Kansy J, Pegoraro M, Quasso F, Zanderighi L. Positron annihilation study of free volume in cross-linked amorphous polyurethanes through the glass transition temperature. *Polymer*. 1998;1:3491-3498. doi:10.1016/s0032-3861(97)10063-5
65. Bartos J, Sausa O, Kristiak J, Blochowicz T, Rössler E. Free-volume microstructure of glycerol and its supercooled liquid-state dynamics. *J Phys Condens Matter*. 2001;30:11473-11484. doi:10.1088/0953-8984/13/50/307
66. Awad S, Abdel-Hady EE, Mohamed HFM, Elsharkawy YS, Gomaa MM. Non-fluorinated PVA/SSA proton exchange membrane studied by positron annihilation technique for fuel cell application. *Polymers Adv Technol*. 2021;20:3322-3332. doi:10.1002/pat.5345

How to cite this article: Uyumaz F, Artuç GÖ, Pehlivan G, et al. Preparation and characterization of an acrylated-coumarin-containing photo-crosslinked thiol-ene network: Investigation of the free-volume, thermal, UV, and photoluminescence properties. *Polym Eng Sci*. 2025;65(4):1949-1960. doi:10.1002/pen.27125